

Reconstruction of Wigner function of electron beams based on coherence measurements

Shuhei Hatanaka^{1,2,*} and Jun Yamasaki^{1,3}

¹*Research Center for Ultra-High Voltage Electron Microscopy,
Osaka University, 7-1 Mihogaoka, Ibaraki, Osaka 567-0047, Japan*

²*Graduate School of Engineering, Osaka University, 2-1 Yamadaoka, Suita, Osaka 565-0871, Japan*

³*Institute of Materials and Systems for Sustainability,
Nagoya University, Furo-cho, Chikusa, Nagoya 464-8601, Japan*

(Dated: April 23, 2024)

We developed a reconstruction method for the density matrix and Wigner function of electron beams through analysis of the Airy pattern intensity profile. The density matrix in a transmission electron microscope object plane was calculated using the coherence function and the electron wave amplitude and phase distributions. The Wigner function was then reconstructed using the matrix elements. Based on the Wigner function at the origin of the phase space, we derived a formula to calculate the axial brightness, and then measured the axial brightness of a Schottky field emission gun, which reflects the emitter performance more accurately and precisely than the conventional mean brightness measurements.

Electron beams are important probes to measure material structures and electronic states on the nanometer scale, particularly in transmission electron microscopes (TEMs). Recently, quantum measurements of electron beams themselves and control of electron states have been realized in TEMs, e.g., controlling electron states via the interaction between free electrons and the optical near field[1], measurement of antibunching of electrons[2], and realization of quantum logic gates for free electrons[3]. The possibility of decoherence measurements of electrons entangled with bulk plasmon and surface plasmon is also proposed[4].

Electrons generated from an electron emitter are in a mixed state[5] that can be expressed using a density operator. The density operator contains all knowable information about the quantum system, including the wave nature e.g., the phase and coherence of the electron waves, which cannot be described via the particle model. For quantum measurements such as decoherence measurements, state measurements based on the density operators before and after the interaction are important.

One alternative way to describe the information contained in the density operator is to use the Wigner function, which describes the state in phase space spanned by the position and momentum bases. When considered in a 2D plane, the Wigner function is given by[6]

$$W(\mathbf{r}, \mathbf{q}) = \frac{1}{(2\pi)^2} \iint_{-\infty}^{\infty} d^2\boldsymbol{\mu} e^{-iq\boldsymbol{\mu}} \langle \mathbf{r} + \frac{\boldsymbol{\mu}}{2} | \hat{\rho} | \mathbf{r} - \frac{\boldsymbol{\mu}}{2} \rangle, \quad (1)$$

where \mathbf{r} and $\boldsymbol{\mu}$ are 2D real space vectors, and \mathbf{q} is a 2D reciprocal space vector. $\hat{\rho}$ is the density operator. It is known that Wigner functions can have negative values as a manifestation of quantum nature, as measured for photons and laser cooled ions in Fock states[7, 8], and matter wave interference[9]. Because of this negative value

characteristic, the Wigner function is a quasiprobability distribution.

The phase space representation of a beam in an optical system can also be derived in a classical manner using ray diagrams, but the Wigner function gives a complete description of the wave field, including the coherence, intensity distribution, and phase distribution in phase space. The Wigner function thus allows evaluation of the power going in each direction at each position in the optical system. Therefore, when compared with the density operator, the Wigner function is advantageous when evaluating the axial brightness in a TEM, which represents the electric current propagating along the optical axis.

In quantum optics, the Wigner function has been reconstructed in various ways e.g., phase space tomography[10, 11], optical homodyne tomography[12], and heterodyne measurement[13]. It is, however, difficult to apply these methods to actual electron waves because of the lack of flexibility of the TEM optical system. To reconstruct the Wigner functions of electron waves, methods based on in-line or off-axis holography in TEMs have been investigated theoretically[14]. However, the limitations on the variable range of the illumination lens system and Fresnel scattering by the biprism cause serious problems when attempting to obtain the correct reconstructions in each method[14].

Here, we propose a method to measure the density matrix based on the Airy pattern from an aperture. Using the matrix elements measured for the electron beams in a TEM, the Wigner function of the electron waves is reconstructed for the first time. In addition, using the reconstructed Wigner function, the axial brightness, which is an important performance indicator for emitters, is measured with greater accuracy and precision than in conventional measurements.

Generally, the diagonal density matrix elements are obtained via intensity measurements, whereas phase measurements are performed to determine the off-diagonal

* hatanaka@uhvem.osaka-u.ac.jp

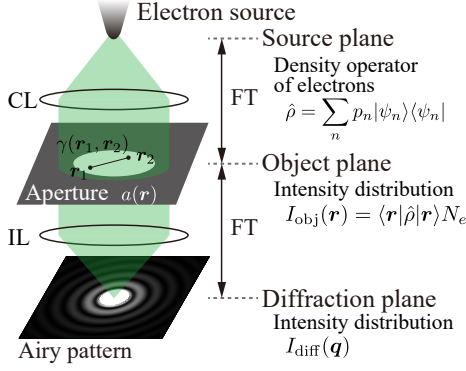


FIG. 1. Simplified drawing of the optical system to form the Airy pattern in a TEM. CL, condenser lens system; IL, imaging lens system; FT, Fourier transform relation; $\gamma(\mathbf{r}_1, \mathbf{r}_2)$, coherence function; $a(\mathbf{r})$, aperture function; $\hat{\rho}$, density operator.

elements. In our previous research, a method to determine the phase distribution in real space via Airy pattern intensity analysis was developed[15]. A simplified drawing of the optical diagram in a TEM to record the Airy pattern is shown in Fig. 1, where the illumination system composed of multiple condenser lenses is denoted by CL, and the imaging system composed of multiple intermediate lenses, a projection lens, and lenses in the energy filter is denoted by IL. As described in [15], the energy filter was used not to eliminate electrons with energy fluctuations but to enlarge the Airy patterns sufficiently to enable precise measurements.

In a TEM, electrons generated by an emitter pass through the CL and then illuminate the object plane. The object plane beam intensity is $I_{\text{obj}}(\mathbf{r}) = \xi(\mathbf{r})^2$, where $\xi(\mathbf{r})$ is the amplitude of the wave field $\Psi(\mathbf{r})$. As Fig. 1 shows, when a circular aperture in the object plane is illuminated using a nearly parallel beam, an Airy pattern appears in the diffraction plane formed by the IL. Because all electron sources have a finite size, then based on the particle model, electrons emitted from different points on the source surface reach the object plane from slightly different directions. Using the wave model, this situation can be expressed as an incoherent superposition of the electrons in different states. The statistical mixture of these different states, i.e., the mixed state is expressed using the density operator $\hat{\rho} = \sum_n p_n |\psi_n\rangle\langle\psi_n|$, where p_n is the probability of the state $|\psi_n\rangle$. To be precise, energy fluctuations between the electrons are also represented by different states, but they do not affect the Airy pattern formed by small-angle scatterings[15]. Therefore, the influence of these energy fluctuations is omitted from the formulation for Airy pattern analysis. In quantum mechanics, a two-point correlation is expressed using $\langle\mathbf{r}_1|\hat{\rho}|\mathbf{r}_2\rangle$ with the normalization $\text{Tr}[\hat{\rho}] = 1$ for \mathbf{r} inside the aperture. In optics, the two-point correlation of a wave field is expressed using the mutual coherence function $\Gamma(\mathbf{r}_1, \mathbf{r}_2) = \langle\Psi(\mathbf{r}_1)\Psi^*(\mathbf{r}_2)\rangle$, where \langle

is the ensemble average[10]. $\Gamma(\mathbf{r}, \mathbf{r})$ is normalized via the integration within the aperture S_a as $\iint_{S_a} d^2\mathbf{r} \Gamma(\mathbf{r}, \mathbf{r}) = \iint_{S_a} d^2\mathbf{r} \xi(\mathbf{r})^2 = N_e$, where N_e is the number of electrons forming the Airy pattern.

When the CL is adjusted ideally to realize the Fourier transform relationship between the emitter plane and the object plane, the parallel illumination $\Psi(\mathbf{r})$ with a uniform amplitude ξ_0 and a uniform phase in the object plane is realized. By considering the difference of the normalization conditions in the mutual coherence function and in the density matrix, the off-diagonal elements of the density matrix are written as

$$\langle\mathbf{r}_1|\hat{\rho}|\mathbf{r}_2\rangle = \Gamma(\mathbf{r}_1, \mathbf{r}_2)/N_e = \gamma(\mathbf{r}_1, \mathbf{r}_2)\xi_0^2/N_e, \quad (2)$$

where $\gamma(\mathbf{r}_1, \mathbf{r}_2) := \Gamma(\mathbf{r}_1, \mathbf{r}_2)/\sqrt{\Gamma(\mathbf{r}_1, \mathbf{r}_1)\Gamma(\mathbf{r}_2, \mathbf{r}_2)}$ is called the coherence function, the absolute value of which represents the degree of coherence[16].

In most practical cases, the illumination beam is not parallel, but is more or less converging/diverging on the object plane, which is expressed as a defocusing effect of the CL. The defocus aberration changes the beam diameter on the object plane, thus causing an increase/reduction of the average amplitude value from ξ_0 . More generally, the amplitude in an actual illumination beam is described as $\xi(\mathbf{r})$, because other aberrations (and other practical reasons, e.g., slight beam misalignment from the optical axis) may induce an amplitude distribution. The actual illumination beam has also the phase distribution induced by the CL aberration, as can be inferred from the fact that a curved wave front is formed in a converging or diverging beam. These phase modulations are generally expressed by applying the unitary operator \hat{U}_{CL} to the electron states. Therefore, the state after the phase shift is expressed using $|\psi'\rangle = \hat{U}_{\text{CL}}|\psi\rangle$. \hat{U}_{CL} has the eigenvalue $e^{-ikX_{\text{CL}}(\mathbf{r})}$ for the position basis; $\hat{U}_{\text{CL}}|\mathbf{r}\rangle = e^{-ikX_{\text{CL}}(\mathbf{r})}|\mathbf{r}\rangle$, where $X_{\text{CL}}(\mathbf{r})$ and $k = 2\pi/\lambda$ are the axial geometric aberration of the CL and the wavenumber given by the wavelength λ , respectively. The density operator after the influence of the lens aberration is expressed by $\hat{\rho}' = \sum_n p_n \hat{U}_{\text{CL}}|\psi_n\rangle\langle\psi_n|\hat{U}_{\text{CL}}^\dagger$. Considering $\hat{U}_{\text{CL}}^\dagger|\mathbf{r}\rangle = e^{ikX_{\text{CL}}(\mathbf{r})}|\mathbf{r}\rangle$ and replacing ξ_0 in Eq. (2) with $\xi(\mathbf{r})$, the off-diagonal elements of the density matrix are calculated using:

$$\begin{aligned} \langle\mathbf{r}_1|\hat{\rho}'|\mathbf{r}_2\rangle &= \sum_n p_n \langle\mathbf{r}_1|\hat{U}_{\text{CL}}|\psi_n\rangle\langle\psi_n|\hat{U}_{\text{CL}}^\dagger|\mathbf{r}_2\rangle \\ &= e^{-ik(X_{\text{CL}}(\mathbf{r}_1) - X_{\text{CL}}(\mathbf{r}_2))} \gamma(\mathbf{r}_1, \mathbf{r}_2) \xi(\mathbf{r}_1) \xi(\mathbf{r}_2) / N_e. \end{aligned} \quad (3)$$

Similar to the way in which the electron waves are modified by the CL aberration before reaching the object plane, a practical Airy pattern is influenced again by the axial geometric aberration of the IL, $X_{\text{IL}}(\mathbf{r})$ [15, 17]. Therefore, the electrons that form the Airy pattern are modulated by the sum of these aberrations: $X(\mathbf{r}) = X_{\text{CL}}(\mathbf{r}) + X_{\text{IL}}(\mathbf{r})$. When the object plane is illuminated via wave packets coming from different source positions,

the Airy pattern is blurred with an angular distribution. The van Cittert–Zernike theorem indicates that the angular distribution has a Fourier transform relationship with $\gamma(\mathbf{r}_1, \mathbf{r}_2)$ [16]. Therefore, the practical Airy pattern intensity is described as[15]:

$$I_{\text{diff}}(\mathbf{q}) = \left| \mathcal{F} \left[a(\mathbf{r}) \xi(\mathbf{r}) e^{-ikX(\mathbf{r})} \right] \right|^2 \otimes \mathcal{F}[\gamma(\mathbf{r}_1, \mathbf{r}_2)], \quad (4)$$

where \mathcal{F} and \otimes represent the Fourier transform and convolution operations, respectively. Combined with a TEM image of the aperture $a(\mathbf{r})$, $\xi(\mathbf{r})$, $X(\mathbf{r})$, and $\gamma(\mathbf{r}_1, \mathbf{r}_2)$ can all be determined simultaneously through fitting

$$W_a(\mathbf{r}, \mathbf{q}) = \frac{1}{(2\pi)^2 N_e} \iint_{-\infty}^{\infty} d^2\boldsymbol{\mu} e^{-i\mathbf{q}\boldsymbol{\mu}} e^{-ik(X(\mathbf{r}+\frac{\boldsymbol{\mu}}{2})-X(\mathbf{r}-\frac{\boldsymbol{\mu}}{2}))} \gamma(\mathbf{r}+\frac{\boldsymbol{\mu}}{2}, \mathbf{r}-\frac{\boldsymbol{\mu}}{2}) a(\mathbf{r}+\frac{\boldsymbol{\mu}}{2}) \xi(\mathbf{r}+\frac{\boldsymbol{\mu}}{2}) a(\mathbf{r}-\frac{\boldsymbol{\mu}}{2}) \xi(\mathbf{r}-\frac{\boldsymbol{\mu}}{2}). \quad (5)$$

The analysis in this paper was conducted using experimental data that were previously reported in [15]. Brief descriptions of the measurement conditions are given as follows. A 200-kV TEM equipped with a Schottky field emission gun (FEG) (JEM-ARM200F, JEOL) was used. A selector aperture (SA) installed in the TEM with an effective diameter of 127 nm at the object plane (Fig. 2(a)) was used to form the Airy patterns. The object plane was illuminated with various beam diameters to vary the spatial coherence inside the aperture from partially coherent to almost fully coherent. The detailed procedures for the measurements and the fitting analysis of the Airy patterns are described in [15].

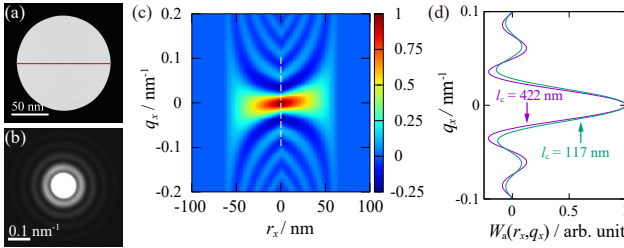


FIG. 2. Reconstruction of the Wigner function. (a) TEM image of the selector aperture. (b) Airy pattern obtained using a beam with coherence length $l_c = 422$ nm. (c) Reconstructed Wigner function $W_a(r_x, q_x)$ calculated from the density matrix along the red line shown in (a). The color bar means the values of $W_a(r_x, q_x)$ with the main peak value normalized to 1. (d) Comparison of the profiles of $W_a(0, q_x)$ along the broken line in (c) for beams with $l_c = 422$ nm and 117 nm. The data of (a) and (b) were measured in [15].

Figure 2(b) shows an example of the measured Airy patterns[15]. Using the parameters determined from Fig. 2(b), the 2D phase space $W_a(r_x, q_x)$ shown in

calculations to the measured Airy pattern based on Eq. (4)[15, 17]. Using the determined $\xi(\mathbf{r})$ and $\gamma(\mathbf{r}_1, \mathbf{r}_2)$, and by replacing $X_{\text{CL}}(\mathbf{r})$ in Eq. (3) with the determined $X(\mathbf{r})$, the off-diagonal elements are then calculated. Note that because of the difference between $X_{\text{CL}}(\mathbf{r})$ and $X(\mathbf{r})$, the result is not for the actual wave in the object plane, but is for a virtual wave that includes the additional phase shift of $kX_{\text{IL}}(\mathbf{r})$. The diagonal elements also can be calculated using Eq. (3) as $\langle \mathbf{r} | \hat{\rho} | \mathbf{r} \rangle = \xi(\mathbf{r})^2 / N_e$. By substituting Eq. (3) as described using $X(\mathbf{r})$ into Eq. (1), the Wigner function reconstructed within the aperture $W_a(\mathbf{r}, \mathbf{q})$ is described using

Fig. 2(c) was reconstructed from the density matrix $\langle r_{x1} | \hat{\rho} | r_{x2} \rangle$ calculated along the 1D line in Fig. 2(a), where r_x is the 1D position basis. The overall shape of $W_a(r_x, q_x)$ shows good agreement with the Wigner function given as the analytical solution for a 1D aperture function[18]. By analogy, from the phase space representation based on ray diagrams and the phase space tomography[10, 11], a slightly tilted crest of high values (shown in red in Fig. 2(c)) around the origin is induced by the curved wavefront in a converging/diverging beam, i.e., by the defocus aberration of the CL. To be precise, the tilted crest is induced by the sum of the defocus aberrations of the CL and the IL. In more general, the overall deformation e.g., slight asymmetric feature in Fig. 2(c) is induced by the other total aberrations of the CL and the IL. Projections of the values of $W_a(r_x, q_x)$ onto the r_x and q_x axes correspond to the intensity profile along the line in Fig. 2(a) and the measured Airy pattern in Fig. 2(b), respectively. The oscillations in both the Airy pattern and $W_a(r_x, q_x)$ are caused by the diffraction phenomenon of the electron waves passing through the aperture. Specifically, the wave (quantum) nature appears in the negative values of $W_a(r_x, q_x)$. Figure 2(d) compares the profiles of $W_a(0, q_x)$ (along the broken line in Fig. 2(c)) reconstructed for beams of different diameters (as explained later, with coherence lengths of $l_c = 422$ nm and 117 nm). The difference in the fringe amplitude compared with the normalized main peak is mainly attributed to the difference in beam coherence.

The brightness is known to be an important indicator of the emitter performance. Specifically, the axial brightness B_0 is of primary importance in optical systems using lenses because the value of B_0 is conserved along the optical axis[19]. B_0 is defined by the electric current passing through an infinitely small area within an infinitely small solid angle along the optical axis, i.e.,

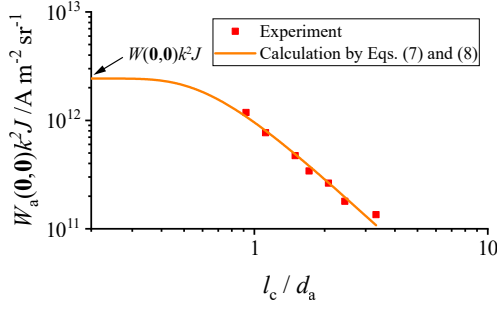


FIG. 3. Electric current at the origin of the phase space $W_a(\mathbf{0}, \mathbf{0})k^2J$ as a function of l_c/d_a . l_c and d_a are the coherence length and the aperture diameter, respectively. The profiles in Fig. 2(d) correspond to the leftmost and rightmost data. The value at $l_c/d_a \ll 1$ corresponds to the axial brightness.

it is defined by the current density at the origin of the phase space [5]. Because small apertures of finite sizes are used in practical measurements[19], the current is measured in an area called emittance that is not infinitely small. Division of the current value by the emittance gives B_0 correctly if the current density within the emittance is uniform, but the value smaller than B_0 in reality because it has a nonuniform distribution with a peak at the origin of the phase space. This is called the mean brightness \bar{B} [19]. Moreover, because the size of the emittance depends on the lens setting and the aperture size used to perform the measurement[19], measured \bar{B} values tend to fluctuate depending on the TEM used and the researchers who conducted the measurements.

Because the Wigner function gives the quasiprobability, B_0 as defined using the current density at the origin of the phase space is given by $W(\mathbf{0}, \mathbf{0})k^2J$ [5], where k^2 is multiplied for the unit conversion from nm^{-2} to sr^{-1} . J is the total electric current in the phase space and, in this work, is equal to the electric current to form the Airy pattern. However, because of the limited integral range in Eq. (5), $W_a(\mathbf{0}, \mathbf{0})$ is different from $W(\mathbf{0}, \mathbf{0})$. Therefore, an appropriate conversion from the measured $W_a(\mathbf{0}, \mathbf{0})$ to $W(\mathbf{0}, \mathbf{0})$ is required to estimate B_0 . From Eq. (5),

$$\begin{aligned} W_a(\mathbf{0}, \mathbf{0}) &= \frac{1}{(2\pi)^2 N_e} \iint d^2\boldsymbol{\mu} e^{-ik(X(\frac{\boldsymbol{\mu}}{2}) - X(-\frac{\boldsymbol{\mu}}{2}))} \\ &\quad \gamma(\frac{\boldsymbol{\mu}}{2}, -\frac{\boldsymbol{\mu}}{2}) a(\frac{\boldsymbol{\mu}}{2}) \xi(\frac{\boldsymbol{\mu}}{2}) a(-\frac{\boldsymbol{\mu}}{2}) \xi(-\frac{\boldsymbol{\mu}}{2}) \\ &\simeq \frac{\xi_0^2}{(2\pi)^2 N_e} \iint d^2\boldsymbol{\mu} a(\frac{\boldsymbol{\mu}}{2}) \gamma(\frac{\boldsymbol{\mu}}{2}, -\frac{\boldsymbol{\mu}}{2}). \end{aligned} \quad (6)$$

A few approximations are used in Eq. (6), as detailed below. It is well known in the electron microscopy field that the main factors of the geometric aberrations in the electromagnetic lenses in a TEM are the defocus aberration, third-order spherical aberration, and first-order astigmatism. The phase shifts induced by the defocus and spherical aberrations are axially symmetric, and that induced by the first-order astigmatism is two-fold rotationally

symmetric with respect to the optical axis[20]. Therefore, the approximation $e^{-ik(X(\frac{\boldsymbol{\mu}}{2}) - X(-\frac{\boldsymbol{\mu}}{2}))} \simeq 1$ holds. Under nearly parallel illumination, the beam intensity inside the aperture can be regarded as being nearly uniform. In fact, based on the fitting results[15], the intensity distribution $\xi(\boldsymbol{r})^2$ inside the aperture is estimated to have deviations of only a few percent. Therefore, considering the circular aperture shape, $a(\frac{\boldsymbol{\mu}}{2})\xi(\frac{\boldsymbol{\mu}}{2})a(-\frac{\boldsymbol{\mu}}{2})\xi(-\frac{\boldsymbol{\mu}}{2}) \simeq a(\frac{\boldsymbol{\mu}}{2})\xi_0'^2$ is a reasonable approximation, where ξ_0' is the average amplitude of the nearly uniform beam inside the aperture. According to the van Cittert-Zernike theorem[16], $\gamma(\frac{\boldsymbol{\mu}}{2}, -\frac{\boldsymbol{\mu}}{2})$ is given by the Fourier transform of the electron source intensity distribution $S(\boldsymbol{q})$, which is generally approximated to be a 2D Gaussian function[15]. As a result, $\gamma(\frac{\boldsymbol{\mu}}{2}, -\frac{\boldsymbol{\mu}}{2})$ can also be approximated to be a 2D Gaussian function, the standard deviation of which is defined as the coherence length l_c . Therefore, $W_a(\mathbf{0}, \mathbf{0})$ in Eq. (6) is given approximately by integration of $e^{-|\boldsymbol{\mu}|^2/2l_c^2}$ within the range determined by the aperture diameter d_a . Using the relationship $N_e = \xi_0'^2 S_a$,

$$\begin{aligned} W_a(\mathbf{0}, \mathbf{0})k^2J &\simeq \frac{k^2 J \xi_0'^2}{\pi^2 N_e} 2\pi \int_0^{\frac{d_a}{2}} d\left(\frac{\mu}{2}\right) \frac{\mu}{2} e^{-\frac{(\mu/2)^2}{l_c^2}} \\ &= B_0 \left(1 - e^{-d_a^2/2l_c^2}\right) \end{aligned} \quad (7)$$

$$B_0 = \frac{k^2 J \xi_0'^2 l_c^2}{2\pi N_e} = 2\pi \frac{J}{S_a} \frac{l_c^2}{\lambda^2} = 2\pi j_0 \frac{l_c^2}{\lambda^2}, \quad (8)$$

where μ and j_0 are the norm of $\boldsymbol{\mu}$ and the axial current density, respectively. The prefactor in Eq. (7) is denoted by B_0 , because $W_a(\mathbf{0}, \mathbf{0})k^2J$ becomes $W(\mathbf{0}, \mathbf{0})k^2J$ if no aperture or an infinitely large aperture is used. In other words, $W_a(\mathbf{0}, \mathbf{0})k^2J$ converges to B_0 when the ratio l_c/d_a approaches zero, as depicted in Fig. 3. B_0 as given by Eq. (8) is a function of j_0 and l_c , which both vary with the CL setting. It was predicted theoretically[21] and confirmed later via our experiments[15, 17] that l_c is a linear function of the beam diameter in the object plane. Considering j_0 is inversely proportional to the square of the beam diameter, the value of $j_0 l_c^2$ and therefore B_0 given by Eq. (8) is constant, regardless of the lens conditions, as expected for the axial brightness characteristics. From the measured values of l_c and j_0 [15], B_0 is estimated to be $(2.5 \pm 0.3) \times 10^{12} \text{ A m}^{-2} \text{ sr}^{-1}$, the precision of which is comes from the measurement errors of the j_0 and l_c values. For reference, \bar{B} values reported previously for the Schottky FEG[22, 23] are in the $(2-10) \times 10^{12} \text{ A m}^{-2} \text{ sr}^{-1}$ range, which is in digit agreement with the present B_0 value. Figure 3 shows the curve for Eq. (7) using the determined B_0 value and the plot of the $W_a(\mathbf{0}, \mathbf{0})k^2J$ values. The good agreement between them verifies the correctness of Eqs. (7) and (8).

The significance of Eq. (8) is that B_0 is expressed using l_c and j_0 , which are intrinsic beam characteristics rather than the emittance, which is affected by the measurement conditions. Interestingly, a similar expression for \bar{B}_p was proposed previously as $\bar{B}_p = 4\pi j_0 l_c^2 / \lambda^2$ [21]. This formula is only valid when an illumination aperture with

a radius of $1/l_c$ is used for the j_0 measurements, unlike Eq. (8), which is free from that aperture size because of much smaller SA than beam diameters. Therefore, if we substitute the same experimental values from Fig. 3 into the formula, \bar{B}_p with twice the value of B_0 is given [17], which is contrary to the general trend noted previously, where $\bar{B} < B_0$. Even if \bar{B} is measured correctly, in addition to the systematic errors caused by the trend, the value fluctuates depending on the TEM and the aperture used, as mentioned earlier. The derived Eq. (8) is an important result that enables electron emitter performance evaluation with high precision and accuracy without being affected by differences in the optical systems.

We have developed a reconstruction method for the density matrix and the Wigner function of electron beams based on Airy pattern intensity analysis. To be precise, the reconstructed Wigner function is not that of the actual wave in the object plane but is that for the wave with the additional phase shift induced by the IL aberration. As shown by the tilted intensity crest caused by the defocus, the wavefront modulations caused by the geometric aberrations appear as overall distortion in the Wigner function. Because only a slight asymmetry appears, the effect of the aberrations is considered to be quite small in Fig. 2(c). Even if the Wigner function contains distortions that cannot be ignored, it is not a problem for application to quantum measurements such as decoherence measurement, in which only the change in the electron states before and after the interaction is important.

Decoherence measurements of inelastically scattered electrons should form one promising application of the developed method. In a previous study, the coherence of electrons inelastically scattered by bulk plasmons

was measured using an electron biprism and an energy filter[24]. As discussed in [17], coherence measurements performed using a biprism present difficulties for poorly coherent electrons such as inelastically scattered electrons because the beam is partly shielded by the biprism itself, settled on the optical axis, but are possible using a specially-fabricated small aperture[17] and the energy filter to select the energy-loss electrons. The decoherence properties of electrons inelastically scattered by surface plasmon and bulk plasmon will be investigated in future studies.

As another important application of the Wigner function, we derived a formula to calculate the axial brightness and then measured the axial brightness of the Schottky FEG precisely and accurately without being affected by differences in the optical system. The ability to estimate axial brightness will be beneficial not only for precise comparison of the performances of various types of electron emitters including photocathodes[2, 25]. Monitoring the degradation process of the emitter performance under various conditions involving vacuum pressure, dark current, and so on should be greatly helpful to obtain the guideline for effective developments of high-performance emitters. The efficiency in developing advanced emitters should be maximized if the present method will be successfully applied not only in TEMs but also in simple vacuum chambers without lenses.

We are grateful for Prof. Y. Nakata of Osaka University and Prof. R. Nishi of Fukui University of Technology for invaluable comments and discussion. This work was partially supported by JSPS KAKENHI grant no. 22K18974, 20K15174, and 26286049.

-
- [1] K. E. Echternkamp, A. Feist, S. Schäfer, and C. Ropers, Ramsey-type phase control of free-electron beams, *Nature Physics* **12**, 1000 (2016).
 - [2] M. Kuwahara, Y. Yoshida, W. Nagata, K. Nakakura, M. Furui, T. Ishida, K. Saitoh, T. Ujihara, and N. Tanaka, Intensity interference in a coherent spin-polarized electron beam, *Physical Review Letters* **126**, 125501 (2021).
 - [3] S. Löffler, T. Schachinger, P. Hartel, P.-H. Lu, R. E. Dunin-Borkowski, M. Obermair, M. Dries, D. Gerthsen, and P. Schattschneider, A quantum logic gate for free electrons, *Quantum* **7**, 1050 (2023).
 - [4] C. Mechel, Y. Kurman, A. Karnieli, N. Rivera, A. Arie, and I. Kaminer, Quantum correlations in electron microscopy, *Optica* **8**, 70 (2021).
 - [5] A. Lubk and F. Röder, Semiclassical TEM image formation in phase space, *Ultramicroscopy* **151**, 136 (2015).
 - [6] E. P. Wigner, On the quantum correction for thermodynamic equilibrium, *Physical Review* **40**, 749 (1932).
 - [7] A. I. Lvovsky, H. Hansen, T. Aichele, O. Benson, J. Mlynek, and S. Schiller, Quantum state reconstruction of the single-photon Fock state, *Physical Review Letters* **87**, 050402 (2001).
 - [8] D. Leibfried, D. Meekhof, B. King, C. Monroe, W. M. Itano, and D. J. Wineland, Experimental determination of the motional quantum state of a trapped atom, *Physical Review Letters* **77**, 4281 (1996).
 - [9] C. Kurtsiefer, T. Pfau, and J. Mlynek, Measurement of the Wigner function of an ensemble of helium atoms, *Nature* **386**, 150 (1997).
 - [10] M. G. Raymer, M. Beck, and D. F. McAlister, Complex wave-field reconstruction using phase-space tomography, *Physical Review Letters* **72**, 1137 (1994).
 - [11] D. McAlister, M. Beck, L. Clarke, A. Mayer, and M. Raymer, Optical phase retrieval by phase-space tomography and fractional-order Fourier transforms, *Optics letters* **20**, 1181 (1995).
 - [12] D. T. Smithey, M. Beck, M. G. Raymer, and A. Faridani, Measurement of the wigner distribution and the density matrix of a light mode using optical homodyne tomography: Application to squeezed states and the vacuum, *Physical Review Letters* **70**, 1244 (1993).
 - [13] K. F. Lee, F. Reil, S. Bali, A. Wax, and J. E. Thomas, Heterodyne measurement of wigner distributions for clas-

- sical optical fields, *Optics Letters* **24**, 1370 (1999).
- [14] A. Lubk and F. Röder, Phase-space foundations of electron holography, *Physical Review A* **92**, 033844 (2015).
 - [15] J. Yamasaki, Y. Shimaoka, and H. Sasaki, Precise method for measuring spatial coherence in TEM beams using Airy diffraction patterns, *Microscopy* **67**, 1 (2018).
 - [16] M. Born and E. Wolf, *Principles of Optics*, 7th ed. (Cambridge University Press, 1999).
 - [17] S. Hatanaka and J. Yamasaki, Quantitative measurement of spatial coherence of electron beams emitted from a thermionic electron gun, *Journal of the Optical Society of America A* **38**, 1893 (2021).
 - [18] A. Torre, *Linear Ray and Wave Optics in Phase Space: Bridging Ray and Wave Optics via the Wigner Phase-Space Picture* (Elsevier Science, 2005).
 - [19] P. W. Hawkes and E. Kasper, *Principles of Electron Optics: Applied Geometrical Optics*, Vol. 2 (Academic press, 1989).
 - [20] R. Erni, *Aberration-corrected imaging in transmission electron microscopy: An introduction*, 2nd ed. (Imperial College Press, 2015).
 - [21] G. Pozzi, Theoretical considerations on the spatial coherence in field emission electron microscopes, *Optik* **77**, 69 (1987).
 - [22] D. B. Williams and C. B. Carter, *Transmission electron microscopy : a textbook for materials science*, 2nd ed. (Springer, 2009).
 - [23] C. J. Humphreys and J. C. H. Spence, Resolution and illumination coherence in electron microscopy, *Optik* **58**, 125 (1981).
 - [24] P. Potapov, H. Lichte, J. Verbeeck, and D. Van Dyck, Experiments on inelastic electron holography, *Ultramicroscopy* **106**, 1012 (2006).
 - [25] S. Hatanaka, T. Tsuchiya, S. Ichikawa, J. Yamasaki, and K. Sato, Ultrafast dynamics of a photoinduced phase transition in single-crystal trititanium pentoxide, *Applied Physics Letters* **123** (2023).